Numerical Investigation of the Viscous Incompressible Flow Around Two Circular Cylinders in Tandem Arrangement

Phan Duc Huynh[*]

Ho Chi Minh City University of Technology and Education
No 1 Vo Van Ngan Street, Linh Chieu Ward, Thu Duc District, Ho Chi Minh City

Abstract

The shedding of vortices and flow interference between two circular cylinders in tandem arrangements are investigated numerically in this paper. The two values 1.5 and 4.0 of the ratio between the distance of two cylinders and the diameter of the cylinder were used. The immersed boundary method (IBM) is used for the simulations of the two-dimensional cases. The calculations are carried out on a Eulerian-Lagrangian grid using the finite difference method. The simulations are performed using two Reynolds numbers 100 and 200. The streamline and vorticity contours of the flow around the cylinders and force time histories are presented. The calculations are also compared to results obtained by other researchers. Numerical results show that the immersed boundary method can easily solve the viscous incompressible flow past single and two cylinders in a tandem arrangement.

Keywords: Immersed boundary method, Circular cylinder, Tandem arrangement, Incompressible flow

1. Introduction

The circular cylinders form the basic component of structures and machinery in the many areas of engineering, for example, cooling towers, heat exchange tubes, cooling systems for nuclear power plants, offshore structures, transmission cables, etc. These structures are immersed in either air or water flow, and therefore they experience flow-induced vibration. This vibration can lead to structural failure under severe conditions. To avoid these situations and to have better structural designs, it is necessary to understand the details of fluid–structure interactions.

There are many investigations on the flow around pairs of circular cylinders [1]. The flow interference that occurs in such configurations is responsible for changes in the fluid loads and in important features of the flow field. In addition, investigations of the flow around pairs of cylinders can provide a better understanding of the vortex dynamics, pressure distribution, and fluid forces in cases involving more complex arrangements. Among the many possible arrangements in which two circular cylinders can be positioned relative to a cross-flow, one that has been extensively studied is the tandem arrangement, as sketched in Fig. 1. In this arrangement, the type of interference presented is wake interference, where the wake of the upstream cylinder touches the downstream one. The effect of this interference is seen, for example, in the variation of the Strouhal number St and

force coefficients with the Reynolds number Re and with the center-to-center distance L.

There are many methods used to simulate flow past two cylinders. The sharp interfaces with an unstructured, triangular mesh to track the motion of arbitrarily complex boundaries [2]; The random - vortex is the approach used in determining velocity and vorticity fields in the proximity of the cylinder and the boundary element method to calculate the pressure [3]. The finite element method with the unstructured grid is most suitable for handling complex flow fields including flow field around multiple cylinders. Usually some suitable cell face center flux reconstruction procedure is devised which incorporates the effect of neighboring cell center velocities and pressures in a more consistent manner. This eliminates the numerical instabilities in course of calculation [4]. In this paper, the immersed boundary method [5] is used to investigate the viscous incompressible flow past two cylinders. In this method, the fluid flow is governed by the incompressible Navier-Stokes equations and these are solved on a stationary Cartesian grid. The structure is represented on a Lagrangian coordinate. The force exerted by the structure on the fluid is calculated by using the Dirac function. This method is fast because the mesh is not resized in each time step. In this paper, the IBM is applied to solve the viscous incompressible flow past over two cylinders which are in a tandem

---

[*] Corresponding author: Tel.: (+84) 909.999.271
Email: huynhpd@hcmute.edu.vn

arrangement. The ratio of the distance between two cylinders and diameter of cylinder *L/D* is 1.5 and 4.0 were used (Fig. 1). The Reynold number of the flow is *Re*=100 and 200.

2. Numerical method

2.1. Immersed boundary method for rigid boundary

We consider the model of problem as a viscous incompressible fluid in a two-dimensional domain Ω_f containing an immersed boundary in the form of a simple closed curve Γ (Fig. 2), the configuration of which will be given in parametric form: $X(s,t)$, $0 \leq s \leq L_b$, $X(0,t) = X(L_b,t)$, where L_b is the length of closed curve Γ, and $X(s,t)$ is a vector function giving the location of points as a function of arc-length, s, and time, t. The boundary is modeled by a singular force, which is incorporated into the forcing density term, f, in the Navier-Stokes equations. The Navier-Stokes equations are then solved to determine the fluid velocity throughout the domain Ω. Since the immersed boundary is in contact with the surrounding fluid, its velocity must be consistent with the no-slip boundary condition. The equations of motion of system are as follows
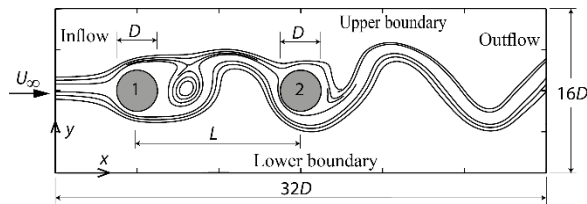
Fig.1. The flow around two cylinders in a tandem arrangement
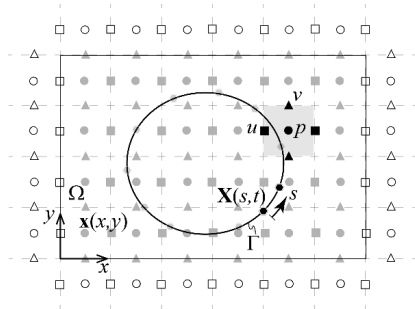
Fig.2. Staggered grid and schematic of the fluid – immersed boundary system

$$\rho \, \partial \mathbf{u}/\partial t + \rho \left(\mathbf{u} \cdot \nabla \right) \mathbf{u} + \nabla p = \mu \Delta \mathbf{u} + \mathbf{f} \qquad (1)$$

$$\nabla \cdot \mathbf{u} = 0 \qquad (2)$$

Here $\mathbf{u}(\mathbf{x},t) = (u(\mathbf{x},t), v(\mathbf{x},t))$ is the fluid velocity and $p(\mathbf{x},t)$ is the fluid pressure, with $\mathbf{x} = (x,y)$ and $\mathbf{X}=(X,Y)$. The coefficients ρ and μ are the constant fluid density and viscosity. The force density acting on the fluid is $\mathbf{f}(\mathbf{x},t) = (f_x(\mathbf{x},t), f_y(\mathbf{x},t))$ which takes the form

$$\mathbf{f}(\mathbf{x},t) = \int_{\Gamma} \mathbf{F}(s,t) \delta(\mathbf{x} - \mathbf{X}(s,t)) ds \qquad (3)$$

where $\mathbf{F}(s,t) = (F_x(s,t), F_y(s,t))$ is the force density at boundary point and $\delta(\mathbf{x}) = \delta(x)\delta(y)$ is the Dirac function. The motion of the boundary is

$$\partial \mathbf{X}(s,t)/\partial t = \mathbf{U}(s,t) = \int_{\Omega} \mathbf{u}(\mathbf{x},t) \delta(\mathbf{x} - \mathbf{X}(s,t)) d\mathbf{x} \quad (4)$$

When simulating the flow around a rigid boundary, we should allow the boundary to move a little bit rather than being fixed. As long as the immersed boundary $\mathbf{X}(s,t)$ stays close to the body surface $\mathbf{X}^e(s,t)$. When the immersed boundary is rigid, the main problem is that the constitutive laws (e.g. Hooke's Law for springs) are in general not well-posed in the rigid limit, meaning that small deformations of a very stiff boundary. One way to deal with this problem is to assume the body to be elastic, but extremely stiff. The forcing term in the equation to make sure that the boundary points will stay close to the body surface, according to Hooke's Law for springs, is written as:

$$\mathbf{F}(s,t) = \kappa \left(\mathbf{X}^e(s) - \mathbf{X}(s,t) \right) \qquad (5)$$

with κ is spring constant. Accurately imposing the boundary condition on the rigid IB requires large values of κ thus it will be chosen so large that the motion will not be noticeable. So if the points on boundary fall away from the desired location, the force of the spring will pull these boundary points back. Thus, as time goes on, we can expect that the boundary points will always be close to their desired configurations.

The force exerted on bodies by the stream comes from the pressure distribution around the bodies and the friction between the stream and the surface of bodies, whose stream-wise component is the drag *D* and the component perpendicular to it is the lift *L*. We can determine the drag and lift force simply by looking at the *x* and *y* component of the force applied by the boundary to the fluid. This, of course, is equal to the negative of the drag, by Newton's third law of motion. Thus,

$$F_D = -\int_{\Gamma} F_x ds \qquad F_L = -\int_{\Gamma} F_y ds \qquad (6)$$

where (F_x, F_y) are the *x*-*y* components of the force **F**.

2.2. Numerical solution approach

2.2.1 Spatial and temporal discretization

The immersed boundary method is a mixed Eulerian-Lagrangian finite difference method for computing the flow interacting with an immersed boundary. An example setup in 2D with a single immersed boundary curve is shown in. Fig. 2. A pair

of computational grids: a cell centered Cartesian grid for Eulerian variables, and a discrete set of points for the Lagrangian variables. Let the fluid domain $\Omega=[0,l_x]\times[0,l_y]$ and $N_x\times N_y$ Eulerian grids, with $h=h_x=h_y=l_x/N_x=l_y/N_y$ is Eulerian grid size. A pair of subscripts on a variable denotes the location at which the Eulerian variable is being evaluated, thus $\mathbf{u}_{ij}$ denotes the value of the variable u at the ij^{th} grid point. We use a set of N_b Lagrangian grid-points (boundary mesh with $\Delta s=L_b/N_b$) and these Lagrangian grid-points are identified by a single index, with variables at such grid-points identified by the corresponding index appearing as a subscript, thus F^k denotes the value of the variable F at the kth grid-point. The location of the kth Lagrangian grid-point is explicitly tracked in X_k. We use a superscript to denote the value of a variable at a given time step; thus $\mathbf{u}^n(\mathbf{x})=\mathbf{u}(\mathbf{x},n\Delta t)$ and $\mathbf{X}^n(s)=\mathbf{X}(x,n\Delta t)$.

2.2.2. Body solver

The force densities are computed at these control points and are spread to the Cartesian grid points by a discrete representation of the Dirac delta function

$$\mathbf{f}_{i,j}^n = \sum_{k=1}^{N_b} \mathbf{F}_k^n(t)\delta_h\left(\mathbf{x}_{i,j}^n - \mathbf{X}_{i,j}^n\right)\Delta s_k \quad (7)$$

where $\delta_h(\mathbf{x})$ is a two-dimensional Dirac delta function,

$$\delta_h(\mathbf{x}) = \phi(x/h)\phi(y/h)/h^2 \quad (8)$$

here ϕ is a continuous function which was derived as

$$\begin{aligned}
\phi(r) &= (3-2|r|+\sqrt{1+4|r|-4r^2})/8, & 0\leq|r|\leq1 \\
\phi(r) &= (5-2|r|-\sqrt{-7+12|r|-4r^2})/8, & 1\leq|r|\leq2 \quad (9)\\
\phi(r) &= 0 & 2\leq|r|
\end{aligned}$$

The Navier–Stokes equations with the forcing terms are then solved for the pressure $p_{i,j}^{n+1}$ and velocity field $\mathbf{u}_{i,j}^{n+1}$ at the Cartesian grid points using finite difference method in a staggered Cartesian grid system. The velocity field is then interpolated to find the velocity at the control points as,

$$d\mathbf{X}_k^{n+1}/dt = \mathbf{U}_k^{n+1} = \sum_{i,j} \mathbf{u}_{i,j}^{n+1}\delta_h\left(\mathbf{x}_{i,j}-\mathbf{X}_k^{n+1}\right)h^2 \quad (10)$$

2.2.3 Navier-Stokes solver

We find the solution at the $(n+1)^{st}$ time step by the following three-step approach:

Treat nonlinear, viscosity and force density terms

We would have a time step restriction proportional to the special discretization squared, so the nonlinear and viscosity terms are treated explicitly,

$$\left(\mathbf{u}^*-\mathbf{u}^n\right)/\Delta t = -\left(\mathbf{u}^n\cdot\nabla\right)\mathbf{u}^n + \mu/\rho\Delta\mathbf{u}^n + \mathbf{f}^n/\rho \quad (11)$$

$$\left(\mathbf{u}^{n+1}-\mathbf{u}^*\right)/\Delta t = -\nabla p^{n+1}/\rho \quad (12)$$

$$\nabla\cdot\mathbf{u}^{n+1} = 0 \quad (13)$$

Pressure correction

We correct the intermediate velocity field $\mathbf{u}^*$ by the gradient of a pressure p^{n+1} to enforce incompressibility, Eq. (12). The pressure is denoted p^{n+1}, since it is only given implicitly. It is obtained by solving a linear system. Applying the divergence ($\nabla\cdot$) to both sides of this equation yields the linear system:

$$\nabla\cdot\mathbf{u}^{n+1}/\Delta t - \nabla\cdot\mathbf{u}^*/\Delta t = -\Delta p^{n+1}/\rho \quad (14)$$

Substituting Eq. (13) into Eq. (14), we have

$$\Delta p^{n+1}/\rho = \nabla\cdot\mathbf{u}^*/\Delta t \quad (15)$$

This is a Poisson equation for the pressure p^{n+1} at the time $(n+1)^{st}$. In summary, the $(n+1)^{st}$ time step consists of the following steps.

Step 1: Compute $\nabla\cdot\mathbf{u}^*$ from the velocity $\mathbf{u}^n$.

Step 2: Solve Eq. (15) for the pressure p^{n+1}.

Step 3: Compute the new velocity field $\mathbf{u}^{n+1}$ using Eq. (12) with the pressure values p^{n+1} computed in Step 2.

Staggered grid

When solving the Navier-Stokes equations, the region Ω is often discretized using a staggered grid, with the pressure p in the cell midpoints, the velocities u placed on the vertical cell interfaces, and the velocities v placed on the horizontal cell interfaces (Fig. 2).

3. Computational problem

The computational domains for the simulations are summarized in Fig. 1. The width of the domain is $32D$. The height of the domain is $16D$. The value of D is 0.1. There are two cases of simulation: single cylinder and two cylinders in a tandem arrangement. The Reynold number of the flow is 100 and 200. For two cylinder case, the ratio of the distance between two cylinders and diameter of the cylinder L/D is 1.5 and 4.0 were studied. The flow velocity is set to $u=1$, $v=0$ at the inlet. On the top and bottom boundaries, a symmetry boundary condition is imposed by setting the normal velocity to zero ($v=0$).

4. Numerical results

4.1 Flow past a single circular cylinder

Flow past an isolated circular cylinder has attractive features like vortex shedding behind the cylinder and the periodic variation of the flow field at

moderate Reynolds number. In the present study, the unsteady flow at $Re = 100$ and 200 are simulated. The size of the grid has been decided based on a grid independence study. Fig. 3 and Fig. 4 show the streamlines and vorticity contours past a single cylinder for $Re = 100$ and 200 respectively at the nondimensional instantaneous time $T=U_\infty t/D=520$. The Karman vortex street is well established in both the cases. Fig. 3 and Fig. 4 also shows the non-dimensional dependent behavior of the drag coefficient ($C_D = 2F_D/(\rho U_\infty^2 D)$) and lift coefficient ($C_L = 2F_L/(\rho U_\infty^2 D)$) on the surface of the cylinder. The clear periodicity illustrated in lift and drag coefficients implies the periodic vortex shedding from the rear surface of the cylinder. Table 1 lists the mean value and amplitude of drag and lift coefficients and Strouhal number ($S_t = fD/(U)$; f is the vortex shedding frequency) of present results as well as the literature results. Comparing with fractional step method [6]; multigrid and preconditioning method [7]; streamfunction-vorticity equations [8, 9]; these results show that the IBM method is an appropriative method for this problem, especially when it is compared with the experiment data [10, 11, 12].

4.2 Flow past two cylinders in tandem arrangement

In order to investigate the proximity effect on vortex shedding, simulations have been carried out for cylinders in tandem arrangements. The Reynolds number for all the simulations is equal to 200. The ratio of the distance between two cylinders and diameter of the cylinder L/D is 1.5 and 4.0 were used. The streamline and vorticity contours are shown in Fig. 5 and 6. The plots in these figures are at the nondimensional instantaneous time $T = 520$ and $T = 1000$, respectively. The wakes are represented by the respective streamline. In Fig. 5, the cylinders act as a single body. There is only one large vortex wake forming behind the downstream cylinder. The downstream body is involved by the separating shear layer from the upstream cylinders. The interaction between these shear layers takes place only in the base region of the downstream cylinder. Comparing the formation distance of an isolated cylinder with the case of the arrangement shown in Fig. 5, it is clearly perceived that in the former the vortex shedding process occurs much closer to the base of the body. The lift coefficient has a small amplitude. The drag coefficient is positive for the upstream cylinder. For the downstream cylinder, it is negative.

In Table 2, the drag and lift coefficients and Strouhal numbers of the cases simulated are shown and compared with those of other researchers. There are no experimental data for verifying the results. There are the different results between the current research and another referencers because of mesh size between two cylinders, the step time, and the size of the domain. For L/D=1.5 the drag coefficient of downstream is negative, indicating that the downstream cylinder is immersed on a low-pressure region formed by the separated shear layers emanating from the upstream body.

Table 1. Summary of results for single cylinder

	Re=100			Re=200		
	C_D	C_L	S_t	C_D	C_L	S_t
Present	1.40±0.015	±0.311	0.162	1.3±0.030	±0.542	0.189
Other results found in the literature						
[6]	-	-	-	1.31±0.04	±0.65	0.20
[7]	1.35±0.012	±0.339	0.164	1.31±0.049	±0.69	0.192
[8]	1.33±0.014	±0.298	0.175	1.17±0.058	±0.67	0.202
[9]	1.38±0.007	±0.300	0.169	1.29±0.022	±0.50	0.195
Experiments						
[10]						0.18-0.2
[11]				1.3		
[12]			0.16-0.17			0.17-0.19

Table 2. Summary of results for two cylinders, $Re = 200$

C_D	C_L	S_t	C_D	C_L	S_t
1.1	0.034	0.166	-0.105	0.087	0.165
1.1121	0.024	0.174	−0.216	0.05	0.174
0.83 ± 0.05	0.2	0.14	−0.17 ± 0.15	0.3	0.14
1.26	0.698	0.174	0.8	1.96	0.174
1.23	0.737	0.18	0.473	1.69	0.18
1.29	0.745	0.19	0.6	1.9	0.19
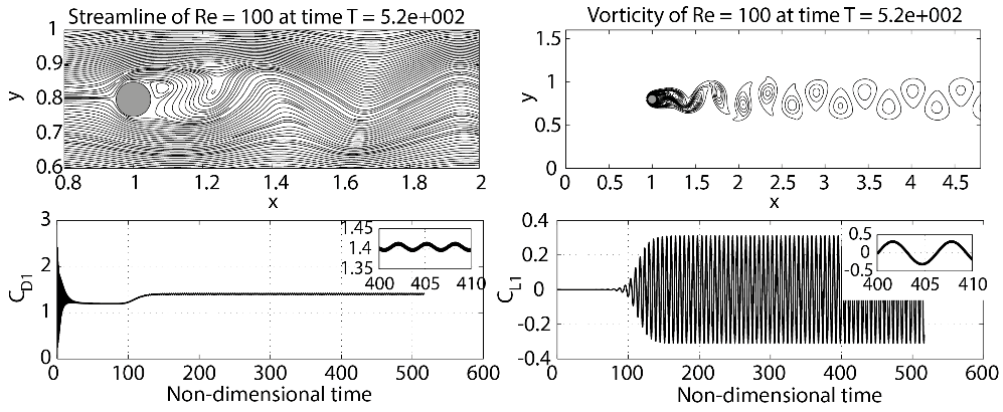
Fig. 3. The flow past single cylinder at *Re* = 100
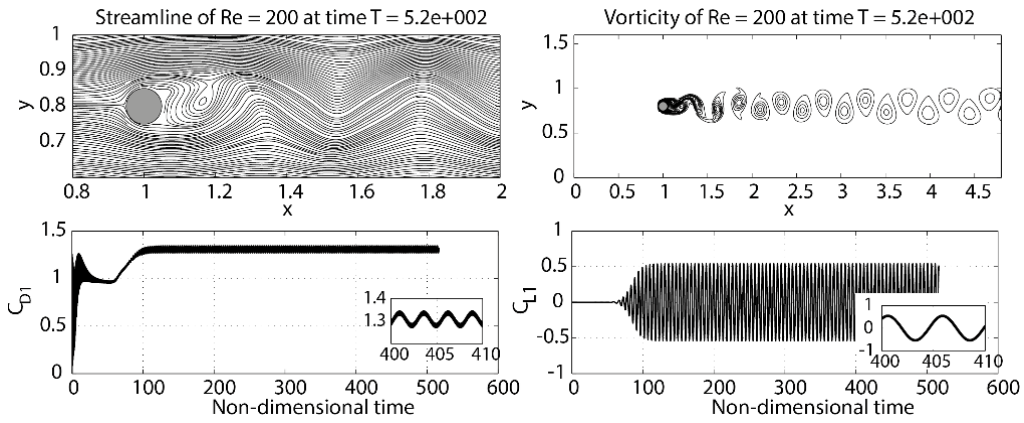
Fig. 4. The flow past single cylinder at *Re* = 200
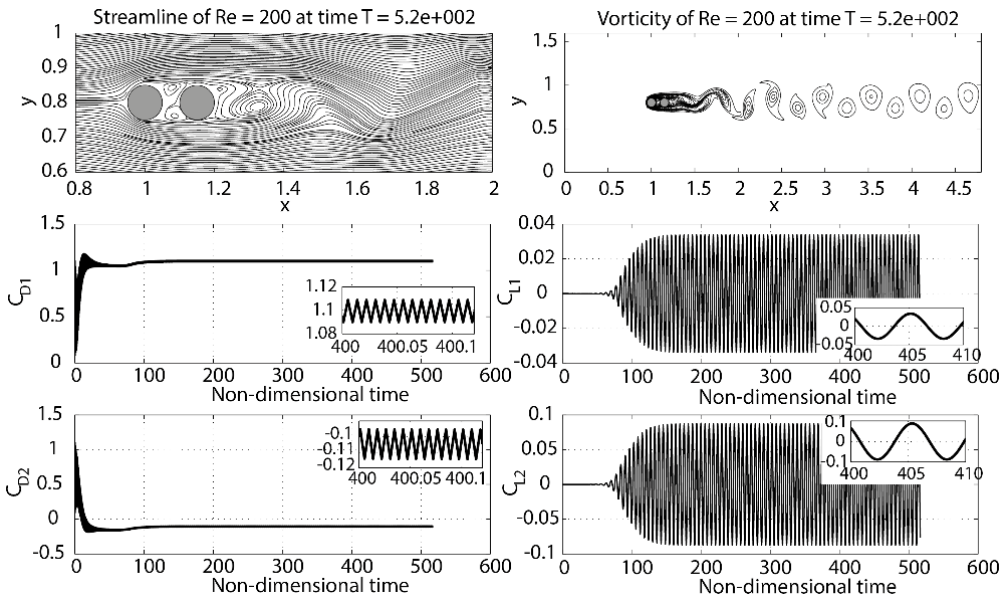
Fig. 5. The flow past single cylinder $L / D = 1.5$
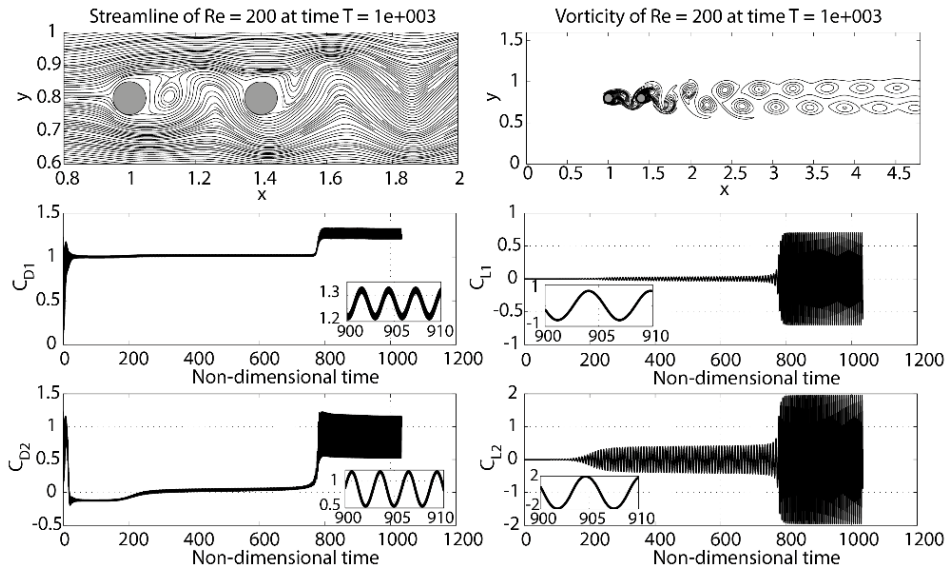
Fig. 6. The flow past single cylinder at $L/D = 4$

The wake visualizations and vorticity contours presented in Fig. 5 corroborates this conclusion. Due to the interference, for the case of L/D=1.5, the Strouhal number is lower than the one found in the case of an isolated cylinder. When the gap is increased from 1.5D to 4D, a very distinct change in the flow characteristics occurs. Fig. 6 shows the results for the gap of 4D. The upstream cylinder starts to shed vortices. The lift coefficients of both cylinders oscillate, with the highest amplitude experienced by the downstream body. The drag of this cylinder becomes positive, even though with an intensity considerably lower than the one from the upstream body. If the gap is further enlarged, the drag on both cylinders increases, suggesting that at higher gaps the result of the drag from an isolated cylinder may be recovered.

5. Conclusions

In this work, the immersed boundary method is used for the calculation of the flow around a single cylinder (Re =100, 200) and two cylinders in tandem arrangement (Re = 200). The streamline and vorticity contours and force coefficient time histories were presented. The results were similar to those observed in the literature. The vortex-induced vibration will be considered in the future to investigate the flow characteristics over vibrational cylinders.

Acknowledgments

References

[1] Y. Zhou, and M. Mahbub Alam, Wake of two interacting circular cylinders. A review. International Journal of Heat and Fluid Flow. 62 (2016) 510-537.

[2] I. Borazjani, and F. Sotiropoulos, Vortex-induced vibrations of two cylinders in tandem arrangement in the proximity-wake interference region. J Fluid Mech. 621 (2009) 321-364.

[3] A. Slaouti, and P.K. Stansby, Flow around two circular cylinders by the random-vortex method. Journal of Fluids and Structures. 6 (1992) 641-670.

[4] K.R. Yu, et al., Flow-induced vibrations of in-line cylinder arrangements at low Reynolds numbers. Journal of Fluids and Structures. 60 (2016) 37-61.

[5] C.S. Peskin, The immersed boundary method. Acta Numerica. (2003) 1-39.

[6] M. Rosenfeld, D. Kwak, and M. Vinokur, A fractional step solution method for the unsteady incompressible Navier-Stokes equations in generalized coordinate systems. Journal of Computational Physics. 94 (1991) 102-137.

[7] C. Liu, X. Zheng, and C.H. Sung, Preconditioned Multigrid Methods for Unsteady Incompressible Flows. Journal of Computational Physics. 139 (1998) 35-57.

[8] D. Calhoun, A Cartesian Grid Method for Solving the Two-Dimensional Streamfunction Vorticity Equations in Irregular Regions. Journal of Computational Physics. 176 (2002) 231-275.

[9] D. Russell, and Z. Jane Wang, A cartesian grid method for modeling multiple moving objects in 2D incompressible viscous flow. Journal of Computational Physics. 191 (2003) 177-205.

[10] J. H. Gerrard, he wakes of cylindrical bluff bodies at low Reynolds numbers. Philos. Trans. R. Soc. Lond. A. 288 (1978) 351–382.

[11] R. Wille, Kármán Vortex Streets. Advances in Applied Mechanics. 6 (1960), 273-287.

[12] A. Roshko, On the drag and shedding frequency of bluff cylinders. Nut. Adv. Comm. Aero., Wash., Tech. Note. (1954) 3169.